

MITIGATION OF SEISMIC POUNDING BETWEEN ADJACENT BUILDINGS BY MEANS OF ISOLATION AND SUPPLEMENTAL DISSIPATION AT THE BASE

F. MAZZA¹ AND R. LABERNARDA²

¹ Dipartimento di Ingegneria Civile, Università della Calabria (Italy)
Ponte P. Bucci, 87036 Rende (CS)
fabio.mazza@unical.it

² Dipartimento di Ingegneria Civile, Università della Calabria (Italy)
Ponte P. Bucci, 87036 Rende (CS)
rodolfo.labernarda@unical.it

Key words: Seismic Pounding, In-Plan Irregular Structures, Single and Double Concave Surface Sliders, Viscous Dampers, Near-Fault Site

Abstract. *Double concave surface slider (DCSS) is considered as an effective solution for base-isolation of existing structures located in a near-fault site, because of its capacity to notably increase horizontal displacements that can be accommodated in comparison to a single concave surface slider (SCSS) of identical in-plan dimensions. However, unexpected torsional pounding of in-plan irregular adjacent structures may be induced by variability of friction force and lateral stiffness of SCSS and DCSS, depending on the axial load and friction coefficient changes during an earthquake. Effectiveness of supplemental viscous damping at the base is studied in this work with the aim to analyse its effectiveness for limiting base displacement, so avoiding too large seismic gap requirement. Structural pounding between fixed-base and base-isolated L-shaped buildings, placed adjacent to form T- and C-shaped plans, is analysed. A simulated design of the original reinforced concrete (RC) fixed-base framed structure is preliminarily carried out in accordance to a former Italian code, for a medium-risk seismic zone. Then, seismic retrofitting with SCSSs is carried out, in order to attain performance levels imposed by the current Italian code in a high-risk seismic zone, while DCSSs have radius of curvature equal to half the SCSSs and the same friction coefficient. The insertion of additional fluid viscous dampers (FVD) at the base is examined, following damping distribution inversely proportional to the distance between the stiffness centre of the base-isolation system and the plane frame where each FVD is placed. Nonlinear modelling of SCSSs and DCSSs considers variable axial load combined with friction coefficient at breakaway and stick-slip and as function of the sliding velocity, axial pressure and rising temperature at the sliding interface. Attention is focused on the pulse-type nature of near-fault earthquakes generally observed in the velocity time-histories but largely overlooked in the acceleration ones. Automated classification algorithms using wavelet analysis are adopted to compile three datasets of seismic input rotated in the range 0°-360°, with a constant step of 15°. Distinction is made between no-pulse and velocity-pulse, the latter further categorised into non-acceleration and acceleration-pulses.*

1 INTRODUCTION

Detrimental effects of seismic pounding between adjacent structures are confirmed by empirical evidences [1]. Experimental studies demonstrated damage on the superstructure caused by seismic pounding at the isolation level [2], while analytical investigations proved floor to floor seismic pounding between base-isolated and fixed-base structures [3,4]. Concave surface sliders (CSSs) can be considered an effective retrofitting solution for reinforced concrete (RC) framed buildings [5], providing coincidence between the gravity mass centre of the superstructure and the stiffness centre of the isolation system. However, numerical studies proved that significant seismic pounding, due to torsional displacements, can be undergone by retrofitted framed building irregular in plan subjected to pulse-type near-fault ground motions, assuming variability of friction force and lateral stiffness of the CSSs as function of axial load, sliding velocity and temperature at the sliding surface [6,7]. Pounding between adjacent fixed-base and base-isolated buildings can be reduced or removed by viscous damper linked at each floor of the superstructure [8,9]. In this work, structural pounding is investigated referring to a RC five-storey L-shaped residential building. Relative displacements between the fixed-base (original) and base-isolated (retrofitted) structures, forming T- and C-shaped plans, are evaluated with the aim of quantifying the effectiveness of supplemental damping at the isolation level, in terms of avoiding pounding. Test structure is designed in accordance with an old Italian code [10] for a medium-risk seismic zone, and retrofitted using single concave surface sliders (SCSS) to satisfy performance levels imposed by current Italian code [11] in a high-risk seismic zone [7]. The retrofitting with double concave surface sliders (DCSS) is also considered, with the latter having radius of curvature equal to half the SCSSs and the same friction coefficient. An advanced model of SCSSs [7] is also implemented for DCSSs, considering variable axial load in combination with friction coefficient at breakaway and stick-slip and as function of the sliding velocity, axial pressure and temperature at the sliding interface. Three types of ground motions are selected from the PEER database [12], categorised into no-pulse and velocity-pulse using wavelet analysis [7], the latter further classified into acceleration and non-acceleration pulse. Finally, all records are rotated from 0° to 360° at steps of 15° .

2 NONLINEAR MODELLING OF THE BASE-ISOLATION SYSTEM

2.1 Single concave surface slider

The mechanical response of a SCSS during the sliding phase contains pendular and friction components that can be evaluated according to equation (1a), where N is the axial load during an earthquake, u_x and u_y represent the horizontal displacements, and a circular biaxial interaction domain is assumed by using the ratio between the hysteretic forces along Y and X direction (θ) (equation (1b)). A gap element with infinitely rigid behaviour in compression is considered in the vertical direction (equation (1c)), with the aim of accounting for the reversal of the axial load from compression to tension depending on the vertical displacement u_v .

$$\mathbf{F}_H = \begin{Bmatrix} F_x \\ F_y \end{Bmatrix} = \frac{N}{R} \begin{Bmatrix} u_x \\ u_y \end{Bmatrix} + \mu N \begin{Bmatrix} \cos \theta \\ \sin \theta \end{Bmatrix}; \quad \theta = \frac{F_{f,y}}{F_{f,x}}; \quad F_V = N \quad u_v \geq 0; \quad F_V = 0 \quad u_v < 0 \quad (1a,b,c)$$

As highlighted by experimental studies [13], friction coefficient (μ) is affected by many parameters: axial load (N), sliding velocity (v), temperature at the sliding interface and the

breakaway and stick-slip phases. An advanced model is implemented for the SCSSs, taking into account the variability of the axial load (N), combined with variable friction coefficient at breakaway and stick-slip and as function of the sliding velocity, axial pressure and temperature [7]. Dependence of the friction coefficient on the axial load (N) and sliding velocity (v) is reported in equation (2) proposed by [14], where: μ_{st} is the static coefficient of friction; μ_{HV} and μ_{LV} are the kinetic friction coefficients at high and low velocity, respectively; α_{dyn} regulates the rate of change of the kinetic friction coefficient with the sliding velocity; α_{st} determines friction coefficient during the transition from the sticking to the sliding phase [15].

$$\mu(N, v) = \mu_{HV}(N) - [\mu_{HV}(N) - \mu_{LV}(N)] \cdot e^{-\alpha_{dyn} |v|} + \left\{ [\mu_{st}(N) - \mu_{LV}(N)] \cdot e^{-\alpha_{st} |v|} \right\} \cdot \frac{|\text{sign}(v) - \text{sign}(u)|}{2} \quad (2)$$

$$\mu_{HV}(N) = A_{HV} \cdot N^{(n_{HV}-1)}; \quad \mu_{LV}(N) = A_{LV} \cdot N^{(n_{LV}-1)}; \quad \mu_{st}(N) = A_{st} \cdot N^{(n_{st}-1)} \quad (3a,b,c)$$

$$f_c(c) = e^{-\left(\frac{c}{c_{ref}}\right)^\gamma}; \quad c(t) = \int_0^t N(t) \cdot |v(t)|^2 dt \quad (4a,b)$$

The quantities μ_{HV} , μ_{LV} and μ_{st} are expressed in terms of the axial load (N) according to equations (3a,b,c), where coefficients A_{HV} , A_{LV} , A_{st} , n_{HV} , n_{LV} and n_{st} are constants determining the rate of change of the friction coefficient with the axial load (N). The influence of temperature at the sliding interface is accounted for multiplying equation (2) by the degradation function f_c defined in equation (4a), where c_{ref} is a parameter regulating the rate of degradation of friction coefficient, γ is a parameter controlling the shape of the function, and c is the degradation variable given by equation (4b) as defined in [14].

2.2 Double surface slider

The double concave surface slider (DCSS) is an adaptation of the SCSS, whose mechanical response, depending on axial load (N) and coefficient of friction (μ), has been defined in Section 2.1. A DCSS consists of two facing concave sliding surfaces, separated by an articulated slider, free to move independently on each other, characterized by radii of curvature R_1 and R_2 and friction coefficients μ_1 and μ_2 , respectively. Under the assumption of radii of curvature large compared to the horizontal displacements, the force-displacement relationship for each sliding surface can be derived as reported in equation (5). All the parameters have the same meaning of Section 2.1, with the clarification that the subscripts 1 and 2 refer to top and bottom concave sliding surfaces, respectively.

$$\mathbf{F}_{H_{1,2}} = \begin{Bmatrix} F_{x_{1,2}} \\ F_{y_{1,2}} \end{Bmatrix} = \frac{N}{R_{1,2}} \begin{Bmatrix} u_{x_{1,2}} \\ u_{y_{1,2}} \end{Bmatrix} + \mu_{1,2} N \begin{Bmatrix} \cos \theta_{1,2} \\ \sin \theta_{1,2} \end{Bmatrix}; \quad \theta_{1,2} = \frac{F_{f,y_{1,2}}}{F_{f,x_{1,2}}} \quad (5)$$

$$u_x = u_{x_1} + u_{x_2}; \quad u_y = u_{y_1} + u_{y_2} \quad (6a,b)$$

$$F_H = F_{H_1} = F_{H_2} \quad (7)$$

It should be noted that total displacements along the X (u_x) and Y (u_y) directions are the sum of the displacements on the top and bottom surfaces (equations (6a,b)), while equilibrium has to be satisfied along the horizontal direction (equation (7)) [16]. An advanced model is considered for DCSSs, assuming friction variability described in Section 2.1 for each sliding surface and using a Quasi-Newton method [17] for the step-by-step solution of the nonlinear system given by (6a,b) and (7).

3 FIXED-BASE AND BASE-ISOLATED TEST STRUCTURES

A RC fixed-base five-storey residential building (Figure 1), representative of a spread typology in Italy [18], is considered as original structure for the numerical investigation. Bays of different length induce in-plan irregularity along both principal directions (Figure 1a); floor height is equal to 4.0 m, for level 1, and 3.3 m, for the other levels, with an overall height of 17.2 m (Figure 1b). One-way ribbed concrete slabs are supported by deep beams; flat beams parallel to the slab direction complete the floor structure.

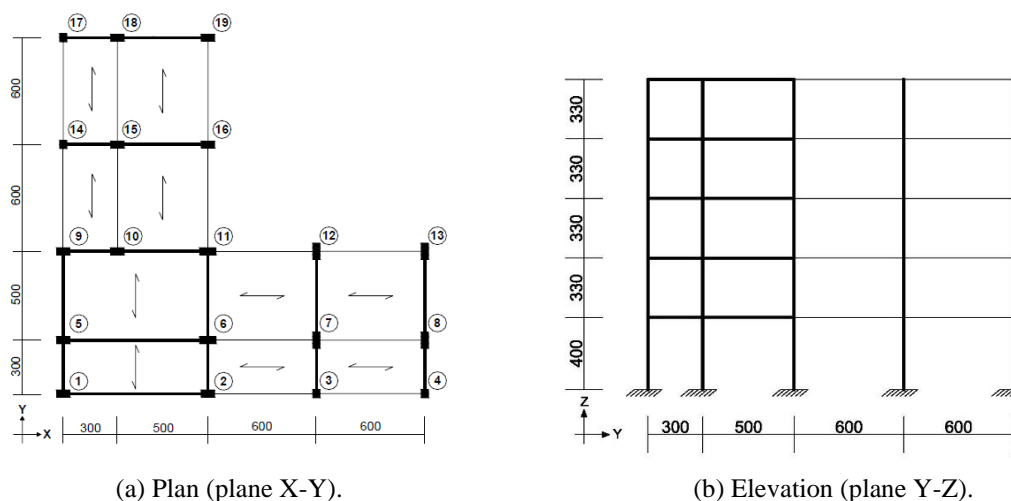


Figure 1: Fixed-base (original) test structure (unit in cm).

A simulated design of the original framed building is performed, at the ultimate limit state, in accordance with an old Italian code [10], for medium-risk seismic region (seismic coefficient $C = 0.07$; response coefficient $R = 1$; structure coefficient $\beta = 1$) and typical subsoil class (foundation coefficient $\varepsilon = 1$). A cylindrical compressive strength of 25 N/mm^2 and a yield strength of 375 N/mm^2 are assumed for concrete and steel, respectively. A dead load of 5.82 kN/m^2 , for the top floor, and 7.12 kN/m^2 , for the other ones, is employed. A live load of 2 kN/m^2 is applied at all levels with an additional snow load of 0.48 kN/m^2 on the roof, considering the latter only for the vertical load combination. Finally, masonry infills regularly distributed in elevation are placed along the perimeter, with an average weight of 1.89 kN/m^2 . The total mass of the building is equal to 1626 t ; main dynamic properties, together with details about cross sections of beams and columns, can be found in [6,7]. A base-isolation system constituted of nineteen SCSSs is assumed for the seismic retrofitting of the original fixed-base building (Figure 2a), attaining performance levels imposed by current Italian code [11] in a

high-risk seismic zone (PGA on rock, $a_g = 0.334 g$ at the CP limit state) and for moderately-soft subsoil (class C, site amplification factor $S = 1.219$). An effective equivalent viscous damping equal to 31.6% is assumed in the horizontal direction ($\zeta_{H,eff}$), neglecting damping in the vertical one. The isolation system is designed on the assumption that the same radius of curvature ($R=4.5$ m) and dynamic friction coefficient ($\mu=4.5\%$) under gravity loads are used for all the isolators, with an effective fundamental vibration period of the isolation system ($T_{iso} = 3.1$ s) depending on spectral displacement at the CP limit state ($d_{dC} = 25$ cm). A new order of rigid beams is placed at the base of the framed structure on the SCSSs (Figure 2b), with an additional mass of the isolation level $m_0=465$ t. Further details can be found in [6,7].

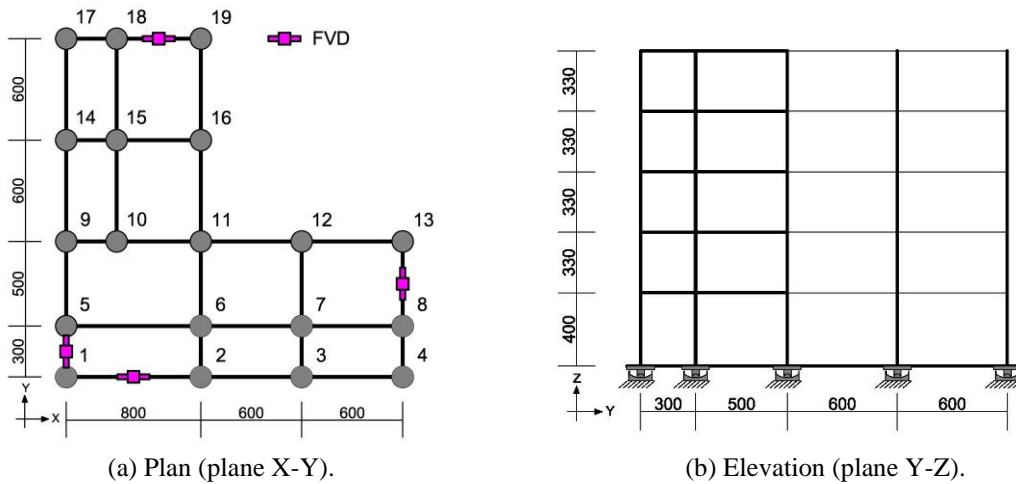


Figure 2: Base-isolated (retrofitted) test structure (unit in cm).

Table 1: Damping properties of FVDs (notation according to Figure 2a)

FVD	Alignment	c (kNs/m)
1	X	328
1	Y	328
13	Y	420
19	X	420

With the aim of analysing the influence of the supplemental damping at the isolation level on limiting displacements, linear fluid viscous dampers (FVDs) are horizontally placed as shown in Figure 2a. The total supplemental viscous damping is evaluated according to a mass-proportional criterion, with an equivalent viscous damping ratio $\xi_{SD}=15\%$, accounting for the fundamental vibration period of the isolation system ($T_{iso} = 3.1$ s) and the overall mass of the base-isolated building $m_{tot}=2091$ t. Then, the damping force of FVDs is distributed inversely proportional to the distance between the stiffness centre of the base-isolation system and the plane frame where each FVD is placed. Damping properties of the selected FVDs are reported in Table 1.

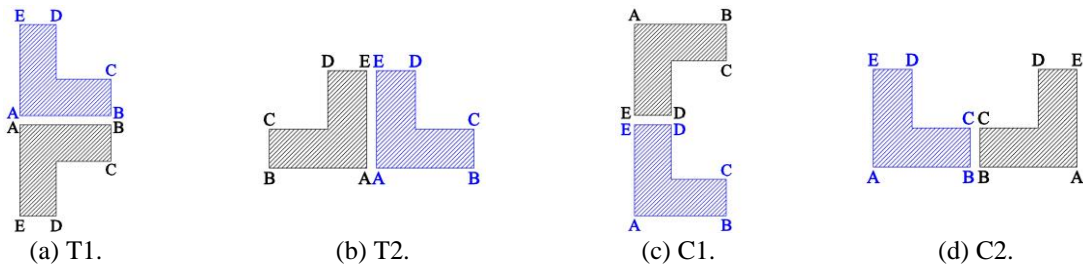


Figure 3: In-plan configurations for adjacent fixed-base (black) and base-isolated (blue) buildings.

Finally, five control points of seismic pounding are monitored (i.e. corners A, B, C, D and E in Figure 3), considering only part of the perimeter exposed to seismic pounding (i.e. sides AB, BC, AE and ED). Attention is focused on aggregation of fixed-base (black) and base-isolated (blue) buildings, with reference to adjacent T-shaped (i.e. T1 and T2) and C-shaped (i.e. C1 and C2) plan configurations.

4 NUMERICAL RESULTS

Nonlinear dynamic analyses of the in-plan irregular RC framed building defined in Section 3, in the original (i.e. fixed-base, Figure 1) and retrofitted (i.e. base-isolated, Figure 2) configurations are carried out considering three typologies of near-fault earthquakes presented in [6,7], rotated into the range 0° - 360° at steps of 15° . Base-isolation systems consist of SCSSs and DCSSs, the latter having radius of curvature equal to half the SCSSs and the same friction coefficient. Relative displacement between fixed-base and base-isolated structures is evaluated with reference to adjacent T- and C-shaped plan configurations (Figure 3), also considering the insertion of FVDs at the isolation level (see Figure 2a). An ad-hoc computer code [19], considering a lumped plasticity model for the nonlinear behaviour of RC frame members, is improved with the aim of accounting for the SCSSs and DCSSs, both designed having the same radius of curvature ($R=4.5$ m) and friction coefficient at high velocity ($\mu_{HV}=4.5\%$) under the gravity loads. An advanced model is considered for SCSSs and DCSSs, with variable axial load combined with friction coefficient variable at the breakaway and stick-slip [15] and depending on sliding velocity, axial pressure and temperature [14]. Parameters for the advanced model are reported in Table 2, with reference to values assumed in [6,7] and with an upper bound threshold for the dynamic friction coefficient equal to 17.05% as suggested by the manufacturer [20]. Shear deformation of RC frame members is neglected, whereas axial and flexural stiffnesses are evaluated using a Young modulus of 31500 MPa. Mass and stiffness proportional damping is assumed, with a viscous damping ratio of 5% and 1% for fixed-base and base-isolated structures, respectively.

Table 2: Parameters of the advanced model for SCSSs and DCSSs

α_{dyn} (s/m)	α_{St} (s/m)	A_{HV}	A_{LV}	A_{St}	n_{HV}	n_{LV}	n_{St}	c_{ref} (kN·m ² /s)	γ
35	350	0.045	0.0225	0.090	0.46	0.37	0.60	4.078E04	0.60

Polar representation of mean values of the relative displacement (g) between fixed-base and base-isolated buildings, at the isolation and roof levels, in the T2 plan configuration is reported in Figure 4, referring to the cases where base-isolation consists of SCSSs (magenta line), SCSSs

combined with FVDs (blue line), DCSSs (green line) and DCSSs combined with FVDs (black line). Note that nonlinear dynamic analyses are carried out considering the same final instant, to take into account early interruption due to tensile uplift of SCSSs and DCSSs, and rotating earthquakes from 0° to 360°. As a comparison, pounding threshold provided by an old Italian code [10] is assumed equal to 20 cm (rounding up the value $H/100$, where H is the total height of the buildings) and represented by a red dashed line.

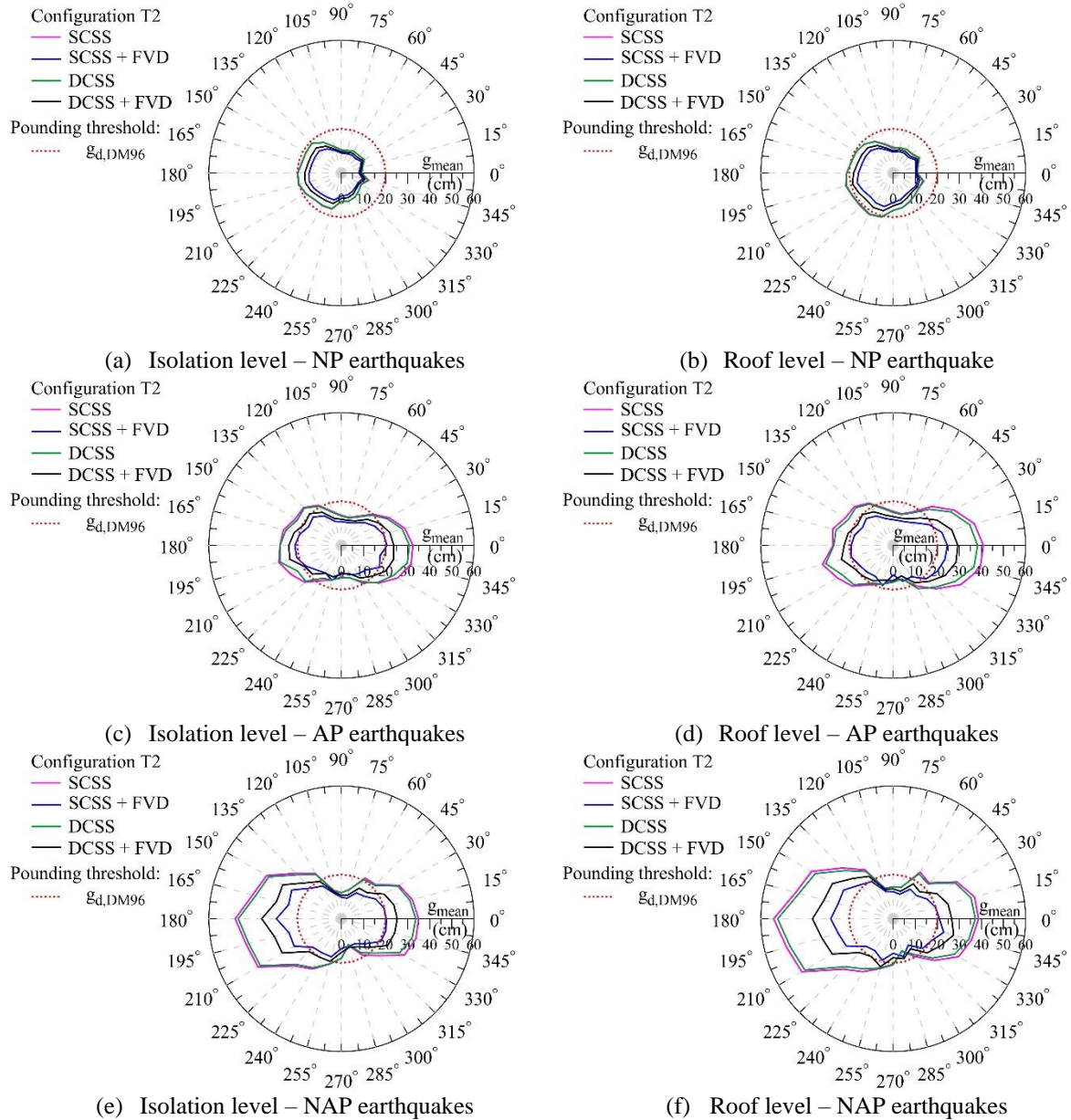


Figure 4: Polar representation of mean values of relative displacement between fixed-base and base-isolated buildings forming T2 shaped plan at the isolation (a,c,e) and roof (b,d,f) levels.

In particular, mean values of the relative displacement (g) at the isolation (Figure 4a) and roof (Figure 4b) levels are depicted in Figures 4a,b, with reference to no pulse (NP) earthquakes. As can be observed, seismic pounding is almost always avoided at the isolation and roof levels for all analysed cases, with only few orientations exceeding DM96 threshold when SCSSs and DCSSs are considered (magenta and green lines respectively). An increase of g is highlighted when acceleration pulse (AP) earthquakes are considered, both at the isolation (Figure 4c) and roof (Figure 4d) levels. Specifically, for an incidence angle of seismic loads falling in the ranges 300° - 45° and 120° - 225° , seismic gap is exceeded for SCSSs (magenta line) and DCSSs (green line), both at the isolation (by about 10 cm) and roof (by about 20 cm) levels, with slightly smaller relative displacement when DCSSs are considered.

Smaller values of g are resulted when SCSSs with FVDs (blue line) and DCSSs with FVDs (black line) are considered, both at the isolation (Figure 4c) and roof (Figure 4d) levels. In particular, combination of SCSSs and FVDs (blue line) proves to be more effective than DCSSs with FVDs (black line) in reducing relative displacement at the isolation and roof levels, exceeding the seismic gap only for few orientations (especially at the roof level). An evident increase in relative displacement and potential seismic pounding can be noted when non-acceleration pulse (NAP) earthquakes are considered, both at the isolation (Figure 4e) and roof (Figure 4f) levels. As can be observed, relative displacement exceeds notably the seismic gap for SCSSs (magenta line) and DCSSs (green line) solutions, reaching a value of about 50 cm especially into the range 120° - 225° . Lower values of g are obtained when SCSSs with FVDs (blue line) and DCSSs with FVDs (black line) are considered, both at the isolation (Figure 4e) and roof (Figure 4f) levels. Specifically, solution with SCSSs and FVDs (blue line) confirms to be more effective than DCSSs with FVDs (black line) in reducing relative displacement between, exceeding the seismic gap only for few orientations (especially at the roof level). Similar considerations can be drawn for other in-plan configurations (Figure 3), not reported for the sake of brevity.

Next, mean values of torsional response (Δ_I) of the base-isolated buildings, defined as the absolute value of the difference between A and B nodal displacements along the Y direction (see Figure 3) are reported in Figures 5a, 6a and 7a along the most critical orientation of NP, AP and NAP earthquakes, respectively. Moreover, time histories of the axial load (N) for the bearing characterized by minimum compression are also plotted in Figures 5b, 6b and 7b. Low torsional response (Δ_I) is recorded for NP earthquakes (Figure 5a), with maximum values of about 5 cm and with slight differences among isolation systems with and without supplemental damping. Almost totally overlapped time histories of axial load (N) can be observed in Figure 5b, referring to CSS#1 (Figure 2a), for the Imperial Valley EQ and seismic orientation $\theta=0^\circ$. It is noteworthy that, in some cases, seismic analyses have been interrupted due to tensile uplift, especially for the SCSSs with and without FVDs.

As shown in Figure 6a, AP earthquakes induce torsional response values (Δ_I) greater than those obtained for NP EQs, with peak values of about 10 cm and an evident difference among the isolation systems with and without supplemental damping. Specifically, SCSSs with FVDs and DCSSs with FVDs highlight lower values of Δ_I compared to those obtained with SCSSs and DCSSs. Almost perfectly overlapped time histories of axial load (N) can be observed in Figure 6b, referring to CSS#1 (Figure 2a), for the Kobe EQ [6,7] and seismic orientation $\theta=60^\circ$.

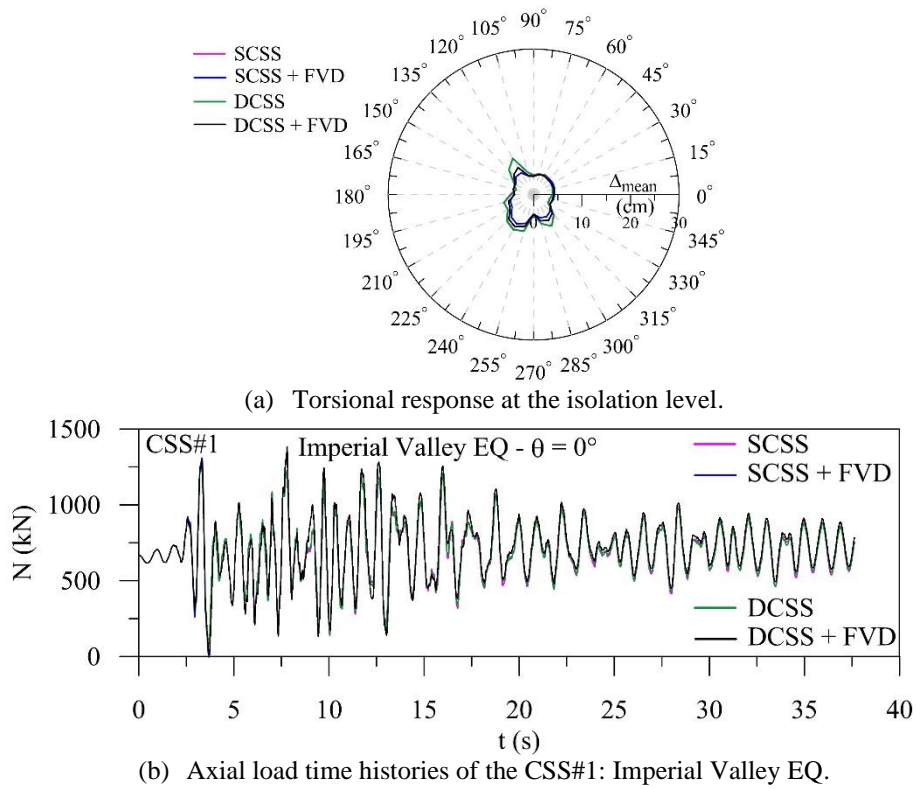


Figure 5: Response parameters for the base-isolated buildings subjected to NP earthquakes.

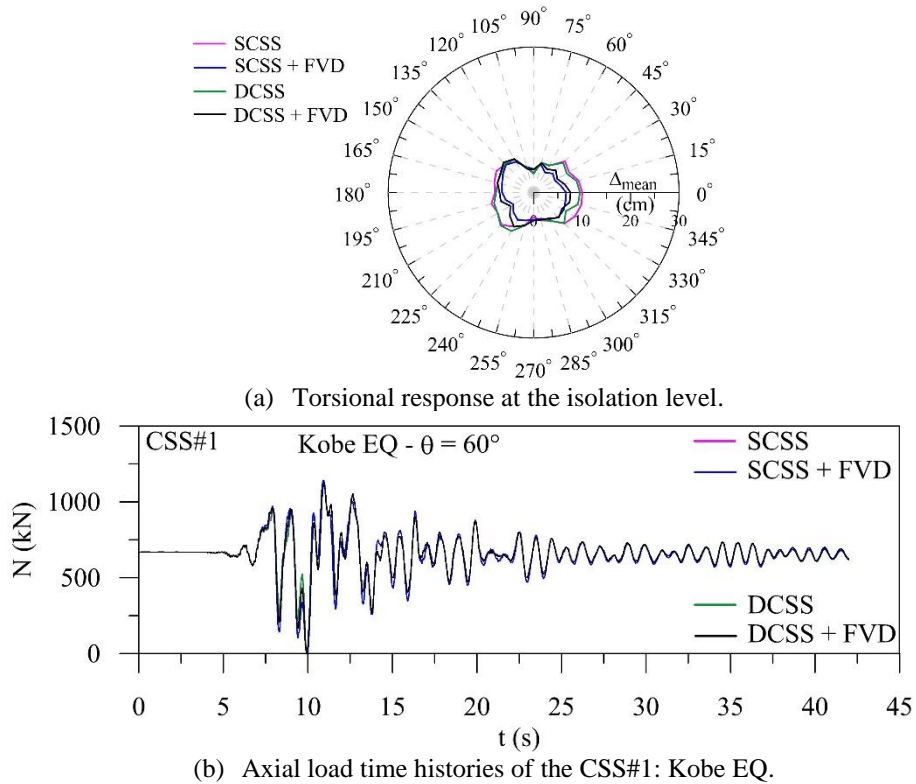


Figure 6: Response parameters for the base-isolated buildings subjected to AP earthquakes.

Finally, considerable values of torsional response (Δt) are resulted in Figure 7a for NAP earthquakes, with maximum values of almost 30 cm and 27 cm for SCSSs (magenta line) and DCSSs (green line) respectively, and notable differences between isolation systems with and without supplemental damping. Specifically, SCSSs with FVDs (blue line) show the lowest values of torsional response with maximum value of about 10 cm, while DCSSs with FVDs (black line) exhibit torsional response with peak values of almost 15 cm. Time histories of axial load for the Duzce EQ highlight that some seismic analyses have been interrupted due to tensile uplift in CSS#1, especially in the SCSSs and SCSSs with FVDs cases compared to DCSSs and DCSSs with FVDs cases (Figure 7b).

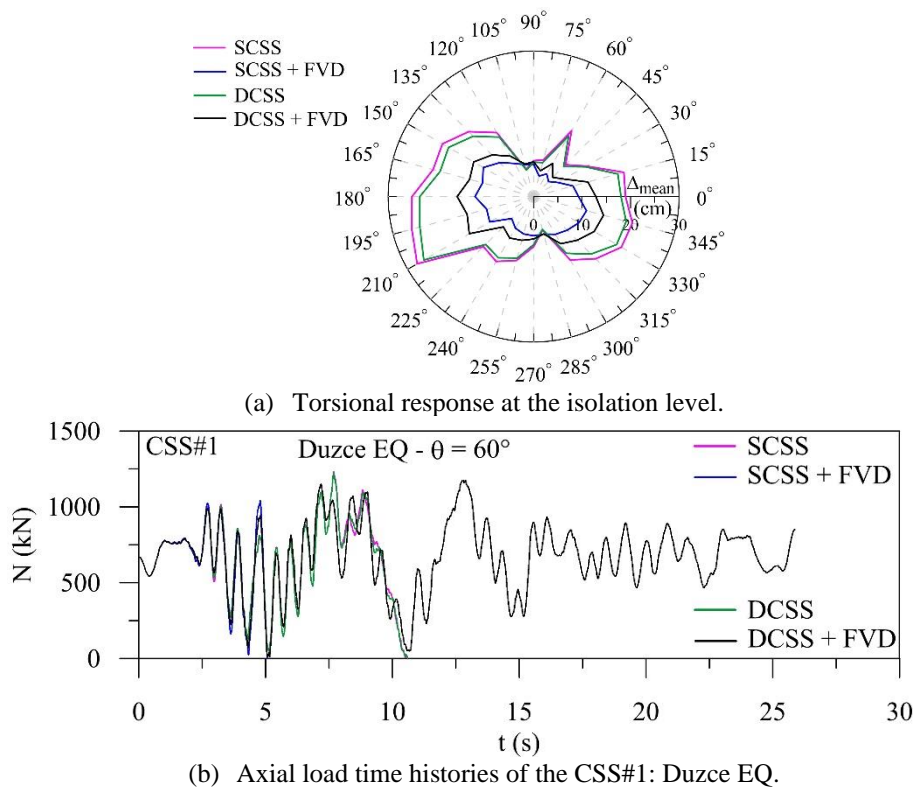


Figure 7: Response parameters for the base-isolated buildings subjected to NAP earthquakes.

5 CONCLUSIONS

Structural pounding is investigated with reference to a RC fixed-base five-storey L-shaped building, considering relative displacements between the fixed-base (original) and base-isolated (retrofitted) structures, ensembled to obtain T- and C-shaped plans. SCSS and DCSS bearings, the latter having radius of curvature equal to half the SCSSs and the same friction coefficient, are assumed with and without considering supplemental damping at the isolation level. An advanced model is considered for SCSSs and DCSSs, accounting for variable axial load and friction coefficient. Three sets of scaled near-fault ground motions, previously categorised as no pulse (NP), acceleration pulse (AP) and non-acceleration pulse (NAP), are rotated into the range 0° - 360° and considered for nonlinear dynamic analyses. Following conclusions can be drawn briefly:

- SCSSs and DCSSs show similar response in terms of relative displacement and torsion when subjected to all typologies of earthquakes;
- notable decrease of relative displacement and torsional response is evident when FVDs are added to SCSSs and DCSSs, with a better performance for SCSSs solution when NAP earthquakes are considered;
- combination of DCSSs and FVDs is the most effective solution in order to avoid tensile uplifting of bearings, representing the best compromise between mitigation of maximum response of the isolation system and seismic pounding.

REFERENCES

- [1] Cole, G., Dhakal, R., Turner, F.M. Building pounding damage observed in the 2011 Christchurch Earthquake. *Earthq Eng Struct Dyn* (2012) **41**:893-913.
- [2] Masroor, A. and Mosqueda, G. Experimental simulation of base-isolated buildings pounding against moat wall and effects on superstructure response. *Earthq Eng Struct Dyn* (2012) **41(14)**:2093-2109.
- [3] Polycarpou, P.C. and Komodromos, P. On poundings of a seismically isolated building with adjacent structures during strong earthquakes. *Earthq Eng Struct Dyn* (2010) **39**:933-940.
- [4] Mazza, F. and Labernarda, R. Internal pounding between structural parts of seismically isolated buildings. *J Earthq Eng* (2021); doi: 10.1080/13632469.2020.1866122.
- [5] Terenzi, G., Fuso, E., Sorace, S., Costoli, I. Enhanced Seismic Retrofit of a Reinforced Concrete Building of Architectural Interest. *Buildings* (2020) **10(11)**:211. <https://doi.org/10.3390/buildings10110211>.
- [6] Mazza, F. and Labernarda, R. Concave Surface Base-Isolation System Against Seismic Pounding of Irregular Adjacent Buildings. *WCCM-ECCOMAS2020*. https://www.scipedia.com/public/Mazza_Labernarda_2021a.
- [7] Mazza, F. and Labernarda, R. Effects of near-fault acceleration and non-acceleration pulses on pounding between in-plan irregular fixed-base and base-isolated buildings. *Struct Control Health Monit.* (2022); e2992. doi:10.1002/stc.2992.
- [8] Mazza, F. and Labernarda, R. Eddy current damped interconnection for mitigation of internal pounding in a seismically-isolated building. *9th ECCOMAS Thematic Conference on Smart Structures and Materials, SMART 2019*, 2019, pp. 1694-1705.
- [9] Mazza, F. and Labernarda, R. Magnetic damped links to reduce internal seismic pounding in base-isolated buildings. *Bull Earthq Eng.* (2020); **18(15)**:6795-6824. doi:10.1007/s10518-020-00961-6.
- [10] DM96. *Norme Tecniche per le costruzioni in zone sismiche*. Ministero dei Lavori Pubblici, D.M. 16-01-1996, (1996).
- [11] NTC18. *Norme Tecniche per le Costruzioni*. Ministero delle Infrastrutture, D.M. 17-01-2018, (2018).
- [12] PEER. *Pacific Earthquake Engineering Research Center database*. (2014).
- [13] Kumar, M., Whittaker, A.S., Constantinou, M.C. Characterizing friction in sliding isolation bearings. *Earthq Eng Struct Dyn* (2014) **44(9)**:1409-1425.
- [14] Gandelli, E., Penati, M., Quaglini, V., Lomiento, G., Miglio, E., Benzoni, G.M. A novel OpenSees element for single curved surface sliding isolators. *Soil Dyn Earthq Eng* (2019) **119**:433-453.

- [15] Quaglino, V., Bocciarelli, M., Gandelli, E., Dubini, P. Numerical Assessment of Frictional Heating in Sliding Bearings for Seismic Isolation. *J Earthq Eng* (2014) **18(8)**:1198-1216.
- [16] Fenz, D.M. and Constantinou, M.C. Behaviour of the double concave Friction Pendulum bearing. *Earth Engng Struct Dyn* (2006) **35**:1403-1424.
- [17] Broyden, C.G. A Class of Methods for Solving Nonlinear Simultaneous Equations. *Mathematics of Computation* (1965) **19(92)**:577-593. <https://doi.org/10.2307/2003941>.
- [18] Mazza, F. Seismic demand of base-isolated irregular structures subjected to pulse-type earthquakes. *Soil Dyn Earthq Eng* (2018) **108**:111-129.
- [19] Mazza, F. and Mazza, M. Nonlinear Modeling and Analysis of R.C. Framed Buildings Located in a Near-Fault Area. *Open Constr Build Technol J* (2012) **6**:346-354.
- [20] FIP Industriale S.p.A. *Catalogo S04: isolatori a superficie curva*. Padova, (2013).